Development of the Zeeman Slower for the Ultra-cold Atomic Interference Experiment

Daniel Gochnauer
Physics REU 2013, Department of Physics, University of Washington

Abstract: The use of atomic interference in ultra-cold atomic physics experiments has become a choice method of studying trapped clusters of neutral atoms. Specifically, this experiment focuses on interference by means of standing light waves with ytterbium Bose-Einstein condensates (BECs) as the atomic source. With the full experimental apparatus, it is expected that high precision measurements, such as those of *h/m* and α, can be obtained. This review reflects the present stage of the experimental set-up, which primarily involves the design, construction, and testing of the Zeeman slower. Some discussion of other electromagnet coils, specifically the MOT coils, will also be included as they are relevant. Not only did the axial magnetic field of the completed slower agree with the predicted field, but the atomic flight simulations also showed the slower to be adequate for experimental use.

I. Introduction:

Over the past decades, experimental atomic physicists have been developing better and better methods for achieving the goals of their experiments. An important theme in experimental atomic physics is the more precise manipulation of the atomic momentum states using light waves [1]. This can lead to diffraction and interference of atomic waves. One of the goals of our new apparatus is to observe this interference phenomenon and take very precise measurements, which can then be used to calculate a precise value of the fine-structure constant. The fine-structure constant, α, can be calculated using atomic physics parameters as follows [2]:

$$\alpha^2 = \frac{2R_\infty}{c}\frac{M}{M_e}\frac{h}{m}, \qquad (1)$$

in which the Rydberg constant, the speed of light in a vacuum, and the mass of an electron are already quite accurately known. Therefore, α can be calculated with high precision if precise measurements of *M* and *h/m* can be obtained experimentally.

One experimental direction shows that such interference experiments are more effective when using a BEC, as opposed to a thermal atomic beam. Notably, BECs are the most coherent atomic source, making them excellent candidates for atomic beam sources. The procedure for obtaining a BEC in this particular experiment employs the general method of slowing an atom beam with a reverse propagating cooling laser, and then capturing the slowed atoms in a trap. The interaction between light and atoms is what makes this procedure possible.

The interactive forces between light and atoms can be separated into photon absorption force and emission force, in which the atom receives a momentum kick of $\hbar k$. In regard to photon emission, the average interactive force is zero because the photons are emitted in random directions, so over many emissions the momentum kicks will cancel out. All of the absorption forces, however, come from the photons from the cooling laser, which is continuously propagating in the same direction. This means that the average absorption force per interaction will be $\hbar k$. Therefore, the observed scattering force can be represented by the average absorption force times the rate at which photons are expected to collide with atoms.

$$F_{scatt} = (\hbar k)\left(\frac{\Gamma}{2}\frac{s}{1+s+4\delta^2/\Gamma^2}\right). \qquad (2)$$

If one assumes constant deceleration, then F_{scatt}, as well as the detuning, δ, must also remain constant. However, the Doppler effect creates a dependence of the observed frequency on the velocity. This requires the use of a spatially varying magnetic field, designed so that the Zeeman effect on the energy levels will continuously balance the changing observed energy of the photons from the Doppler effect [3]. Thus, the constant δ must be defined as follows:

$$\delta = \delta_{lab} + \vec{k}\vec{v} + \frac{\overrightarrow{\mu_B}\,\vec{B}}{\hbar}\,. \qquad (3)$$

Furthermore, because these calculations all condense into one dimension, the vector notations can be dropped and this equation can be solved algebraically.

For this particular design, the coherent laser light is set to be on resonance at the beginning of the slower, so the ideal axial magnetic field from the Zeeman slower can be calculated to be,

$$B(z) = B_{max}\left(1 - \sqrt{1 - \frac{z}{L}}\right), \qquad (4)$$

where L is the overall slower length. This equation describes what is commonly referred to as an increasing field slower.

II. Slower Design:

The design of the Zeeman slower consisted of calculating the summation of the axial magnetic field due to individual rings of wire at varying diameters and positions along the beam axis. The magnetic field produced by this assumption can be generalized by,

$$B(z) = \sum_{j=1}^{l}\sum_{i=1}^{n_j}\left(\frac{\mu_0 I}{d_j}\right)\Big/\left(1 + \left(\frac{2\,z_i}{d_j}\right)^2\right)^{3/2}, \qquad (5)$$

for each i^{th} ring at position z_i up to n_j number of rings, for each j^{th} layer of rings at diameter d_j up to l number of layers. Using this process, an optimized geometric design was created to match the ideal field in Equation 4 as closely as possible.

There were, however, some other considerations to be kept in mind. First, the wire, though approximated as individual rings, is in actuality sets of helical coils. This fact was accounted for during the construction of the slower. Also, another factor which was determined in consideration of the construction was that the number of layers for each set of coils had to be an even integer, so that the lead wires would all protrude from the same side. This makes for a geometrically more logical design, as well as minimizing the undesired magnetic field produced by the lead wires.

The geometric design had to be within the limitations of the rest of the apparatus. This includes dimensions such as the overall length of the slower, as well as the largest diameter allowed by the coils at the widest end. These constraints were determined simply by the fact that some space will be taken up by other components of the apparatus. The radial constraint was not an issue for the placement of coils creating the field following the ideal curve; however, the size of the incorporated compensation coils was limited by this restriction.

Another consideration, then, was that which led to the incorporation of the compensation coils into the design. Unlike the ideal axial magnetic field curve, the real magnetic field would not drop instantly back to zero. The problem which arises is that the peripheral field extends into the magneto-optical trap (MOT), where it is desirable to have zero magnetic field and no additional gradient from the slower coils [4]. Therefore, compensation coils producing an opposing magnetic field can be placed at a large radius and close to the trap center on the same side as the Zeeman slower, diminishing the undesired effect.

It was determined to be in the best interest to include an offset magnetic field in the final design. The purpose of this magnetic field offset was, essentially, to try to increase the quantity of atoms in the trap, as well as increasing the rate at which atoms might be trapped. Ordinarily, without an offset field,

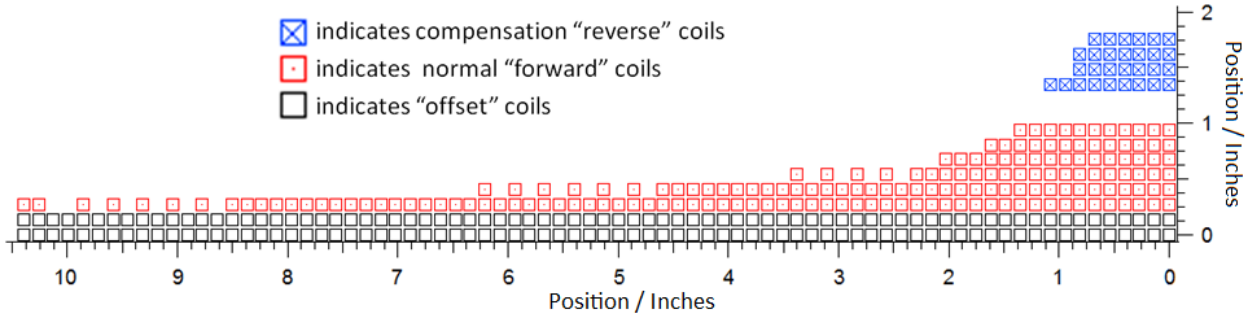

Figure 1. Radial cross-section schematic of the final design for the Zeeman slower
Note: The position on the *y*-axis is the location relative to the surface of the pipe which the wire was wound around.

there is a certain maximum velocity for which atoms can be successfully trapped, so given an initial velocity distribution, only the fraction of atoms moving at less than this velocity are expected to be captured. The effect of an offset magnetic field, however, is that within the space before the slower, the laser will be on resonance with atoms of a higher velocity class, shifting them into the capture velocity range by the time they reach the slower [5]. With this method it is likely that atoms will be trapped at both higher quantities and rates.

A profile of the final geometric design is shown in Figure 1.

III. Construction:

For the construction of the electromagnetic coils of the Zeeman slower, a unique type of wire was used. The wire was copper, for high conductivity, square, for ease of wrapping, hollow, for water-cooling purposes, and insulated with Kapton, a material that can withstand baking at high temperatures. The dimension of the hole was 1/16 inches square. The outer dimension of the copper wire was 1/8 inches square; however, including insulation, the outer dimension was 0.135 inches square [6]. The wire was to be wound around a pipe made of brass, due to its relatively low electrical conductivity. The brass pipe is about 10.6 inches in length, has an outer diameter of 1.00 inch, and has an inner diameter of 0.87 inches.

The Zeeman slower coils were hand-wound on a lathe, using several specific techniques which were developed during the winding process. Prior to winding the first layers, some preparations had to be made, which would contribute to making the process much smoother. An aluminum backstop was machined to fit over the brass pipe, which was, at this point, still three feet in length. Kapton paper and Kapton tape were then used to cover the pipe and the backstop, to prevent the wire from coming in direct contact. This assembly was then put on the lathe, with the backstop at one end. Next, two pieces of wood with a square groove cut in the middle were fashioned to form a track through which the wire would be fed. This square track served to keep the wire from twisting, while also maintaining a sufficient tension to keep the wire from unwinding.

After securing the wooden track in the tool holder on the lathe, winding of the first two layers commenced. The subsequent sets of layers were wound in groups of two, four, two, and four layers respectively. (The final set of two layers simply acted as a support for the four reverse layers above them. These were not included in Figure 1, as they will not contribute to the magnetic field.) For the beginning of each set, the lead wire was held with a hose clamp to keep from slipping,

using ample protection to prevent damage of the wire. Similarly, because the wire was hollow, it was important that the wire not be bent too severely or else pinching might occur. Because a lathe was being used, it was beneficial to utilize the auto-feed feature, which moved the tool holder an axial distance proportional to the angular rotation. All leads were cut to about 1 meter in length and were tied up temporarily along the excess brass pipe. Thermally conductive epoxy was applied periodically throughout the entire winding process, and then applied liberally again at the end. After everything was dry, the leads were straightened out, the pipe was cut short, and aluminum backstop was removed.

Before proceeding much further, the wires were briefly checked, ensuring that there were no electrical shorts or pinched waterlines.

IV. Data and Simulations:

The axial magnetic field was measured through the length of the remaining brass pipe using an axial Hall probe. The probe had a plastic guide attached to it, which held it in the center of the brass pipe. The axial magnetic field profile was measured for three different cases: the 'forward' coils, as labeled in Figure 1, the 'reverse' coils, and the 'offset' coils. The idea behind this was that various linear combinations of these field profiles can be compared and further optimized, in terms of the current that will be put through each set of coils.

Figure 2 shows the three individual axial magnetic field profiles, for the forward, reverse, and offset layers of coils. In addition to these data, a magnetic field profile was also measured for the case where the forward and reverse coils were running simultaneously. This acted as a check against the relative positions of the individual data sets. As shown in Figure 3, both the 'simultaneous' measured field and the linear combination of individual fields fit the calculated field profile very well. Additionally, Figure 3 displays the expected magnetic field which had been calculated prior to any measurements. It can be seen then, that the measured magnetic field agreed quite precisely with the predicted field.

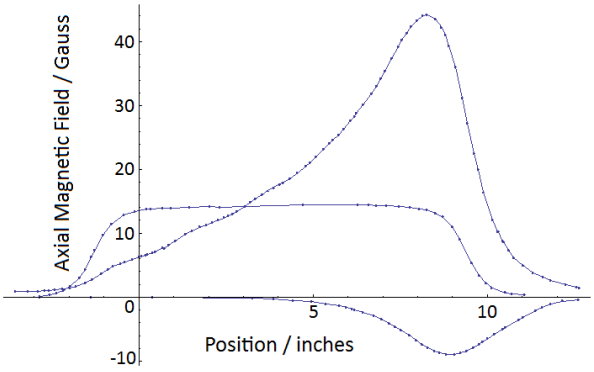

Figure 2. Individual data sets for Forward, Reverse, and Offset coils
Experimental conditions: Forward at 3.00A, 0.625V; Reverse at 3.00A, 0.358V; Offset at 2.00A, 0.275V

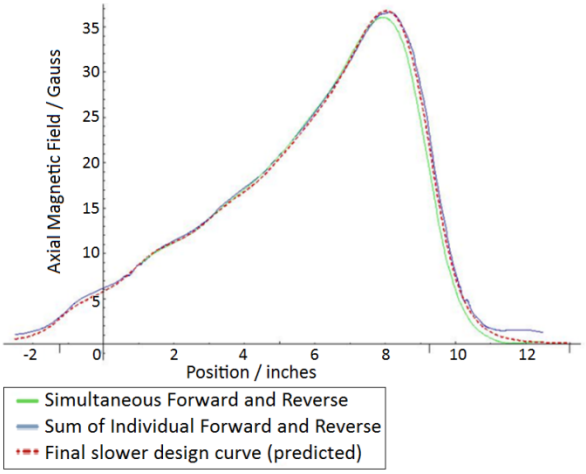

Figure 3. Comparison of measured field profiles with calculated field profile
Experimental conditions: Simultaneous forward and reverse at 3.00A, ~1.2V

Interpolating functions were created for each of the four sets of measured data. These were then used to run various simulations of ytterbium atoms in the environment of the apparatus. All of the following simulations are calculated from a linear combination of the interpolating functions for the individual forward, reverse, and offset magnetic fields.

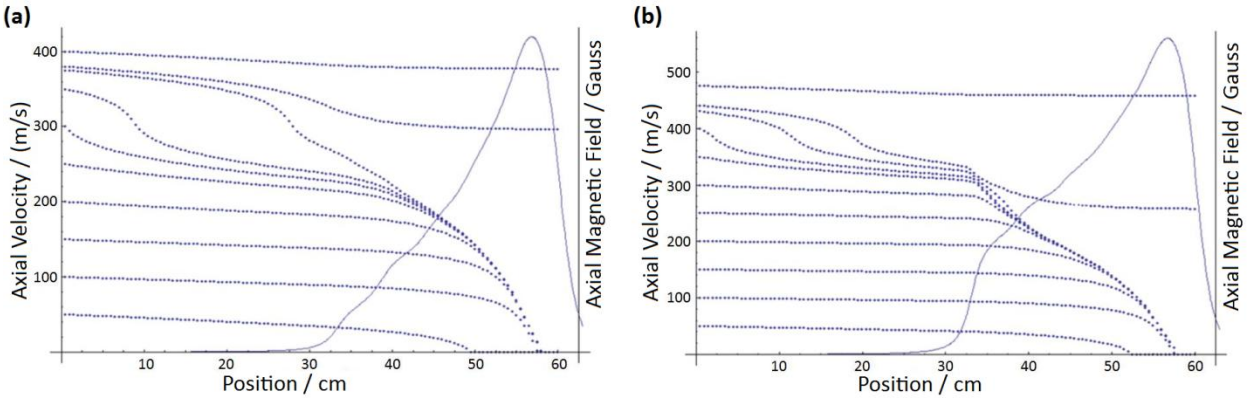

Figure 4. Flight simulations, showing the effect of the offset field
Simulation conditions: (a) Forward and Reverse coils at 35A, I/I_{sat} at 10, Offset coils at 0A, and zero laser detuning, (b) Forward and Reverse coils at 35A, I/I_{sat} at 10, Offset coils at 20A, and laser detuning at -7 linewidths.

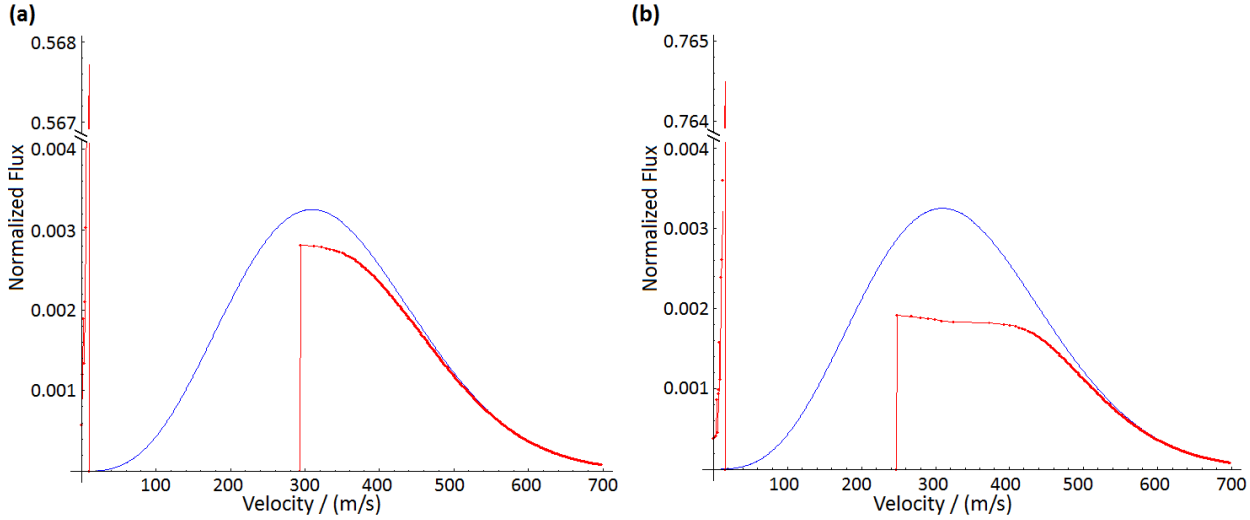

Figure 5. Calculated velocity distributions of flux, showing the effect of the offset field
Simulation conditions: (a) Forward and Reverse coils at 35A, I/I_{sat} at 10, Offset coils at 0A, zero laser detuning, and oven temperature at 674K, (b) Forward and Reverse coils at 35A, I/I_{sat} at 10, Offset coils at 20A, laser detuning at -7 linewidths, and oven temperature at 674K.

The atomic flight simulations were used to show the velocity of a particular atom as it travels through space. In Figure 4, the flight simulations are shown for various initial velocities for two different scenarios. The magnetic field profile is overlaid on the same graph, at its respective, relative position. In both graphs, the slower coils end at 60cm, and therefore begin at about 33.3cm. From the design of the overall apparatus, the ytterbium atoms would leave the oven at 0cm, so there is about 33.3cm of space over which the atoms travel before they reach the magnetic field of the slower. This is the cause of a notable feature in these plots: the additional deceleration due to the partially on-resonant cooling of higher velocity classes in the space between the oven and the Zeeman slower.

Another feature to note is that for each scenario there is a certain capture velocity, as predicted from the equations. However, the predicted capture velocity is calculated as the velocity at the beginning of the slower coils, so the off-resonance cooling may actually allow for a higher true capture velocity. Also, as expected, the offset magnetic field further increases the capture velocity, by the mechanism described in Section II.

When initial velocity of ytterbium atoms is considered as a Maxwell-Boltzmann distribution, it is possible to predict the fraction of captured atoms from the respective probabilities of each initial velocity. Moreover, it would be possible to construct a rough probability distribution of the final velocities, or in other words, a normalized graph of atomic flux versus the velocity. Two final velocity distributions are shown in Figure 5, representing the same two scenarios as in Figure 4. Integrating the sharp peak of low nonzero velocities gives the fraction of atoms which are within that velocity range at the end of the slower. Figure 5a shows the final velocity distribution for zero offset field, and the peak integral was calculated to be 0.64. In Figure 5b, there exists a specified offset field, and the peak integral was calculated to be 0.75. Again, the offset field worked as predicted. The same calculations had been done using the ideal magnetic field curve, and these reported results were within 2% of the predicted values.

V. Conclusions:

In this study, an understanding of basic atomic physics allowed for the development of some experimental equipment, which is intended for use in much more in-depth endeavors. The production of the desired equipment, however, was a successful one. The magnetic field measurements all fit very well with the predicted magnetic field profile. The atomic flight simulations and the final velocity distributions based on the measured data also matched the predictions based on the simulations using the calculated magnetic field. Additionally, the qualitative effect of the offset field was as expected, even prior to predictive calculations. As mentioned earlier, it would be logical from this point to run a series of simulations to optimize the linear combination of forward, reverse, and offset magnetic field profiles.

A similar procedure is also expected to be carried out with a pair of anti-Helmholtz MOT coils. At the present stage of the experimental set-up, the MOT coils have been designed and prepared for construction. A profile in the same style as Figure 1 would yield a simple rectangle, 5 coils wide and 6 layers high. The diameter which the innermost coils will be wrapped around is 3.4 inches. These dimensions would produce a calculated gradient of 0.54G/cm/A. After construction, measurements can be taken and verified in the same fashion as those for the Zeeman slower.

On the scale of a longer timeline, it is the goal that the completed apparatus will be used to run various atomic physics experiments, particularly those regarding or related to atomic interference.

VI. Acknowledgements:

This work was supported by funding from the National Science Foundation and by facilities made available through University of Washington's INT and Physics REU summer research opportunity, as well as assistance from Dr. Subhadeep Gupta's research group.

References:

[1] Gupta, S., Leanhardt, A.E., Cronin, A.D., and Pritchard, D.E. (2001). Coherent manipulation of atoms with standing light waves. *C. R. Acad. Sci. Paris*, **4**, 1–17.

[2] Gupta, S., Dieckmann, K., Hadzibabic, Z., and Pritchard, D.E. (2002). Contrast interferometry using Bose-Einstein condensates to measure *h/m* and *α*. *Physical Review Letters*, **89**, 140401.

[3] Foot, C.J. (2005). *Atomic Physics*. Oxford University Press, 178-217.

[4] Chu, S. (1998). The manipulating of neutral particles. *Rev. Mod. Phys.*, **70**, 685.

[5] Mayera, S.K., Minarik, N.S., Shroyer, M.H., and Mclntyre D.H. (2002). Zeeman-tuned slowing of rubidium using σ+ and σ- polarized light. *Optics Communications*, **210**, 259.

[6] Maloney, N. (2008). *Magnetic coils for ultracold atom control*. Walla Walla University.